Key Points:
- We show that ammonia can melt water-ice crystals in Jupiter's storms and lead to the formation of water-ammonia hailstones (mushballs)
- These mushballs and subsequent downdrafts transport ammonia to very deep levels
- This can potentially explain Juno measurements that Jupiter's ammonia abundance is variable until at least 150 km below the visible clouds

Correspondence to:
T. Guillot,
tristan.guillot@oca.eu

Storms and the Depletion of Ammonia in Jupiter: I. Microphysics of "Mushballs"

Tristan Guillot[1,2] [ID], **David J. Stevenson[3]** [ID], **Sushil K. Atreya[4]**, **Scott J. Bolton[5]** [ID], and **Heidi N. Becker[6]** [ID]

[1]Université Côte d'Azur, OCA, Lagrange CNRS, Nice, France, [2]Department of Earth and Planetary Science, The University of Tokyo, Tokyo, Japan, [3]Division of Geological and Planetary Sciences, California Institute of Technology, Pasadena, CA, USA, [4]Climate and Space Sciences and Engineering, University of Michigan, Ann Arbor, MI, USA, [5]Southwest Research Institute, San Antonio, Texas, USA, [6]Jet Propulsion Laboratory, California Institute of Technology, Pasadena, CA, USA

Abstract Microwave observations by the Juno spacecraft have shown that, contrary to expectations, the concentration of ammonia is still variable down to pressures of tens of bars in Jupiter. We show that during strong storms able to loft water ice into a region located at pressures between 1.1 and 1.5 bar and temperatures between 173 and 188 K, ammonia vapor can dissolve into water ice to form a low-temperature liquid phase containing about one-third ammonia and two-third water. We estimate that, following the process creating hailstorms on Earth, this liquid phase enhances the growth of hail-like particles that we call mushballs. We develop a simple model to estimate the growth of these mushballs, their fall into Jupiter's deep atmosphere, and their evaporation. We show that they evaporate deeper than the expected water cloud base level, between 5 and 27 bar depending on the assumed abundance of water ice lofted by thunderstorms and on the assumed ventilation coefficient governing heat transport between the atmosphere and the mushball. Because the ammonia is located mostly in the core of the mushballs, it tends to be delivered deeper than water, increasing the efficiency of the process. Further sinking of the condensates is expected due to cold temperature and ammonia- and water-rich downdrafts formed by the evaporation of mushballs. This process can thus potentially account for the measurements of ammonia depletion in Jupiter's deep atmosphere.

Plain Language Summary The Juno mission has revealed that Jupiter's atmosphere is much more complex and intriguing than previously anticipated. Most of Jupiter's atmosphere was shown to be depleted in ammonia. While ammonia was expected to be well mixed, large scale variability of ammonia was detected at least 100 km below the cloud level where condensation occurs. We propose a mechanism to explain this depletion and variability. We show that in Jupiter, at very low temperatures (of order −90° C), water ice and ammonia vapor combine to form a liquid and we hypothesize that this subsequently triggers unexpected meteorology. During Jupiter's violent storms, hailstones form from this liquid, similar to the process in terrestrial storms where hail forms in the presence of supercooled liquid water. Growth of the hailstones creates a slush-like substance surrounded by a layer of ice, and these "mushballs" fall, evaporate, and continue sinking further in the planet's deep atmosphere, creating both ammonia depletion and variability, potentially explaining the Juno observations.

1. Introduction

Ammonia condenses in Jupiter's atmosphere at pressures lower than about 0.8 bar and would be expected to be uniformly mixed below that level (Atreya et al., 1999). Ground-based VLA radio-wave observations have shown that, in several regions of the atmosphere, ammonia is depleted down to at least several bars (de Pater et al., 2016, 2019). Microwave radiometer (MWR) observations from Juno (Bolton et al., 2017; Li et al., 2017) show that the depletion extends throughout the midlatitudes, is variable, and is much more prevalent than previously reported, reaching very deep levels: At midlatitudes, the volume mixing ratio of ammonia remains relatively low (between about 120 to 250 ppmv) until it increases to a value ~360 ppmv at pressures greater than 20–30 bars. In the northern component of Jupiter's equatorial zone, at latitudes between 0 and 5°N, the mixing ratio is relatively uniform vertically and equal to ~360 ppmv. Such a global change in ammonia abundance cannot be explained solely by meridional circulation because it would violate mass
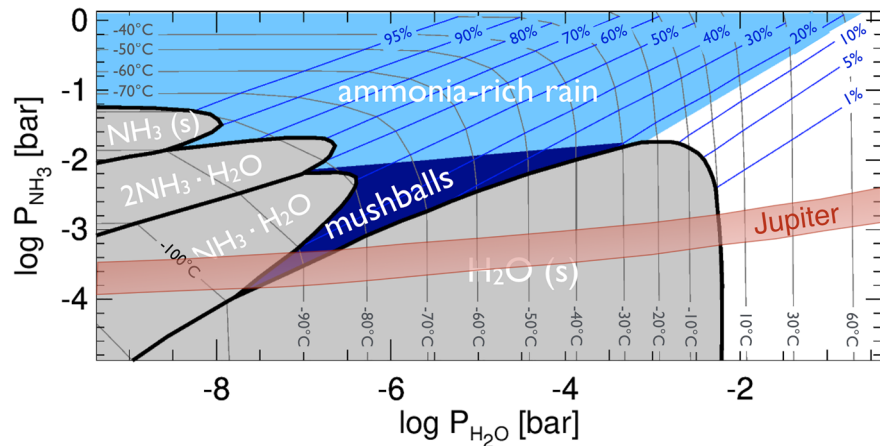
Figure 1. H_2-NH_3 equilibrium phase diagram (Weidenschilling & Lewis, 1973) as a function of partial pressure of H_2O and NH_3. Solid phases are indicated in gray, otherwise, a liquid mixture forms with a concentration in ammonia indicated by the blue diagonal contour. The temperatures in celsius are indicated as contour lines running from the bottom to the left of the plot. The red region labeled Jupiter corresponds to Jupiter's atmosphere assuming a minimum NH_3 abundance of 100 ppmv and a maximum value of 360 ppmv (Li et al., 2017).

balance (Ingersoll et al., 2017). A local depletion of ammonia down to 4–6 bars may be explained by updrafts and compensating subsidence (Showman & de Pater, 2005), but this process cannot extend much deeper below the water cloud base and is thus unable to account for the Juno measurements.

We propose a scenario that can account for the observed vertical and latitudinal dependence of the ammonia concentration. In this paper, we show that during strong storms, ammonia in Jupiter can dissolve into water-ice crystals at temperatures around −90°C, subsequently leading to the formation of partially melted hailstones that we call "mushballs," and to their transport to great depths. In a second paper, we will apply this scenario to explain the Juno MWR measurements.

In section 2, we first investigate the interaction between ammonia vapor and water-ice crystals. We then calculate in section 3 the growth and transport of the "mushballs" thus formed. We discuss in section 4 how further downward transport of ammonia- and water-rich gas must result from evaporative cooling and subsequent downdrafts.

2. The Interaction Between Ammonia Vapor and Water-Ice Crystals

2.1. The NH$_3$-H$_2$O Phase Diagram

Ammonia is known to dissolve easily into liquid water, a consequence of similar dielectric properties of the two molecules. This has been recognized early on (Lewis, 1969; Weidenschilling & Lewis, 1973) and led to the current models of Jupiter's cloud structure, which state that at pressures levels between 2 and 9 bars, depending on the H_2O abundance, a water-cloud layer is formed, and some ammonia is dissolved into liquid water droplets forming a weak aqueous ammonia solution cloud (Atreya et al., 1999). The amount dissolved is however small: At −20°C (corresponding to a ~4 bar pressure level in Jupiter) equilibrium chemistry predicts that a maximum of only 3% of ammonia can dissolve into supercooled liquid water droplets (Ingersoll et al., 2017). Deeper in the atmosphere, at higher temperatures, ammonia solubility decreases while at higher elevations water freezes and should not include any significant amount of ammonia. Given the solar O/N ratio of 7.2 (Lodders, 2003), it is difficult to imagine how rainstorms could affect in any significant way the ammonia budget (Ingersoll et al., 2017).

However, in the same pioneering article about Jupiter clouds, John S. Lewis states the following:

"It is not as commonly known that the freezing point of aqueous NH$_3$ can be depressed as low as −100.3°C, and that the solid phases formed upon freezing of concentrated NH$_3$ solution can be NH$_3$·H$_2$O or 2NH$_3$·H$_2$O, not necessarily solid NH$_3$ or H$_2$O."

In Figure 1, we reproduce the NH_3-H_2O phase diagram of Weidenschilling and Lewis (1973), showing solid phases in gray (from left to right, NH_3 ice, $2NH_3 \cdot H_2O$ ice, $NH_3 \cdot H_2O$ ice, and H_2O ice) and liquid $NH_3 \cdot H_2O$ in white and blue colors. The solid $NH_3 \cdot 2H_2O$ phase discovered later—see Kargel (1992)—is not included, but will not affect the results of the present work. The concentration of ammonia in the aqueous solution decreases from left to right from over 95% in the upper left to less than 1% in the lower right. Using the pressure temperature profile $P(T)$ measured in Jupiter by the Galileo probe (Seiff et al., 1998) and a given volume mixing ratio x_{NH_3} of ammonia, we can readily calculate the partial pressure of ammonia as a function of temperature in Jupiter, that is, $P_{NH_3}(T) = x_{NH_3}P(T)$. The result for x_{NH_3} between 100 and 360 ppmv, the approximate range of ammonia mixing ratios measured by Juno (Li et al., 2017) is shown as a red ribbon in Figure 1.

Let us follow the upward motion of a water droplet formed below the 5-bar level in Jupiter's deep atmosphere by following the red ribbon in Figure 1 from right to left. As liquid, it can dissolve a small fraction of ammonia—but this fraction remains smaller than a percent in equilibrium conditions and reaches a few percent only by invoking large supercooling of the water droplets to −20°C or so, as obtained by Ingersoll et al. (2017). When the droplet freezes to become an ice crystal, the equilibrium solution predicts the existence of pure water ice, implying that any ammonia must be expelled. However, when moving still higher up, in a region between 173 and 188 K (i.e., −100°C to −85°C), equilibrium chemistry predicts that a liquid $H_2O \cdot NH_3$ mixture with a 30%–40% concentration of ammonia should form. Although this was recognized early on, this possibility was never really considered for Jupiter because of the fast rainout of water droplets and ice crystals (Atreya et al., 1999; Lewis, 1969; Weidenschilling & Lewis, 1973). However models of water thunderstorms including detailed microphysics show that storms are able to loft 100 ppmv of water ice to the 1 bar level in the form of 10- to 100-μm particles (Yair et al., 1995). Storms so large that they can reach the stratosphere have been observed and modeled as extended water storms (Hueso et al., 2002; Sugiyama et al., 2014). These storms can last for up to about 10 days. They are believed to carry most of the intrinsic heat flux of the planet (Gierasch et al., 2000).

Thus, although on average the abundance of water near the 1-bar level in Jupiter's atmosphere is extremely small, during large storms, conditions are met for the presence of a significant amount of ice in a region in which liquid $NH_3 \cdot H_2O$ may form. On Earth, hail grows most rapidly in the presence of supercooled liquid water (Pruppacher & Klett, 1997)—it is thus possible that on Jupiter, large storms lead to the formation of large $NH_3 \cdot H_2O$ condensates and their fall to deeper levels. Because the concentration in ammonia can be large, up to 40%, this is a mechanism that can potentially deplete ammonia from the upper atmosphere more efficiently than it depletes water. Interestingly, at even higher levels (pressures lower than 1.2 bars), the equilibrium phase is a solid $NH_3 \cdot H_2O$ condensate with an even higher ammonia concentration (up to 50%).

We name these condensates "mushballs" because we expect the presence of both solid and liquid phases containing variable amounts of ammonia and water and because the liquid phase thus formed is a highly viscous "mush" (Kargel et al., 1991). Now let us examine whether they have time to form and grow.

2.2. Adsorption of Ammonia Into Water-Ice Particles

Large thunderstorms on Jupiter can loft small-size (∼10–100 μm) ice particles up to regions near a pressure of 1 bar (Yair et al., 1995). These storms develop over timescales of hours to days (Hueso et al., 2002). Can ammonia be efficiently adsorbed into these water-ice particles on these timescales?

Let us consider an icy H_2O particle that reached a level where equilibrium chemistry (Figure 1) predicts the formation of a $NH_3 \cdot H_2O$ liquid solution (e.g., ∼1.5 bar, $T \sim$ −85°C for a vapor concentration of NH_3 $x_{NH_3} \sim$ 300 ppmv). An estimate of the timescale to melt the particle is obtained by dividing the number of H_2O molecules in the particle to the NH_3 vapor collision rate. Because the mean free path of ammonia vapor $\lambda_{NH_3} \sim 3D_{NH_3}/v_{th} \sim 0.1\ \mu m$ ($D_{NH_3} \sim 0.3$ cm²/s is the diffusion coefficient of ammonia in hydrogen and $v_{th} \sim 1.2 \times 10^5$ cm/s is the average gas velocity for this pressure level in Jupiter—see Table B1) is much smaller than the size of the particles that we consider (10–100 μm), the process is limited by diffusion effects. Given the small terminal velocity of the ice crystals (see Figure 2 hereafter), they can be considered as co-moving with the gas. In this case, the timescale for the melting of an ice crystal by adsorption of ammonia vapor is (Davidovits et al., 2006)

$$\tau_{\text{ads}} = \frac{1}{36} r_{\text{NH}_3 \cdot \text{H}_2\text{O}} a_{\text{Kn}} \frac{\widetilde{\rho}_{\text{H}_2\text{O}}}{\mu_{\text{H}_2\text{O}}} \sqrt{\frac{\mu_{\text{NH}_3}}{\mu}} \frac{\mathscr{R}T}{x_{\text{NH}_3} P} \frac{\widetilde{d}^2}{D_{\text{NH}_3}} \approx 6 \left(\frac{\widetilde{d}}{100\ \mu m} \right)^2 \text{s}, \tag{1}$$

where $r_{\text{NH}_3 \cdot \text{H}_2\text{O}} \sim 1/2$ is the ratio of NH_3 to H_2O molecules of the equilibrium mixture, $a_{\text{Kn}} \sim 0.75$ results from an empirical fit (Davidovits et al., 2006), $\widetilde{\rho}_{\text{H}_2\text{O}}$ is the physical density of ice grains, $\mu_{\text{H}_2\text{O}}$ and μ_{NH_3} are the molar masses of H_2O and NH_3 molecules, respectively, $\mu \sim 2.3$ g/mol is the mean molar mass of the atmosphere, $x_{\text{NH}_3} \sim 300$ ppmv is the molar abundance of NH_3, P is pressure (~ 1.5 bar), T temperature (~ 188 K), $\mathscr{R}$ the gas constant, and $\widetilde{d}$ is the ice grain diameter. Following measurements in Earth's clouds (Pruppacher & Klett, 1997), we adopt $\widetilde{\rho}_{\text{H}_2\text{O}} \sim 0.3$ g/cm³, but admittedly, this parameter is extremely uncertain.

While short, this timescale is longer by $(a_{\text{Kn}}/2)(\widetilde{d}/\lambda_{\text{NH}_3}) \sim 375(\widetilde{d}/100\ \mu m)$ compared to a kinetic timescale (Davidovits et al., 2006). Experiments show that ammonia adsorption by ice crystal in vacuum is imperfect, that is, the so-called uptake coefficient ranges between $\alpha \sim 3 \times 10^{-4}$ to 4×10^{-3} at temperatures between 170 and 190 K (Jin & Chu, 2007; Kasper et al., 2011). This could lead to a timescale one to two orders of magnitude higher than the above one. However, our situation is different because of melting. Based on liquid-droplet-train experiments (Davidovits et al., 2006), we expect in that case values of α much closer to unity, implying that adsorption should be limited by diffusion.

Other limitations include the fact that only the partial pressure of NH_3 above saturation contributes to the adsorption, and the fact that molecules at the surface must diffuse into the interior. The first effect is estimated from the distance to the pure H_2O ice curve in Figure 1 to lead to a limited increase of timescale (decrease of partial vapor pressure) by a factor ~ 2 across the mushball formation region. The latter is linked to the diffusion time scale inside the grain: $\tau_{\text{diff}} \sim \widetilde{d}^2/\widetilde{D}_{\text{NH}_3}$, where $\widetilde{D}_{\text{NH}_3}$ is the diffusion coefficient for NH_3 inside the grain.

Let us consider diffusion of ammonia vapor through the liquid $\text{NH}_3 \cdot \text{H}_2\text{O}$ surface layer. At room temperatures, $\widetilde{D}_{\text{NH}_3}^{\text{liq}} \sim 10^{-5}$ cm²/s, but we must account that it is a strong function of temperature. Laboratory measurements show that the viscosity of the liquid $\text{NH}_3 \cdot \text{H}_2\text{O}$ mixture increases by up to three orders of magnitude at $T = 176.2$ K (Kargel et al., 1991) compared to room temperature. Owing to the Einstein relation, we expect a comparable decrease of the diffusion coefficient, that is, yielding $\widetilde{D}_{\text{NH}_3}^{\text{liq}} \sim 10^{-8}$ cm²/s in our case. This implies that small ice crystals of 10 μm sizes can be melted in ~ 100 seconds but that larger 100-μm crystals could take up to several hours to melt completely if they are compact. The melting time should be significantly shorter if the water-ice crystals are porous.

We thus expect adsorption in the mushball-formation region to be limited by diffusion effects so that $\tau_{\text{ads}} \sim 100 \left(\widetilde{d}/10\ \mu m \right)^2$ s. Assuming a 50 m/s updraft, 100 s corresponds to the expected crossing-time of the ~ 5-km mushball-formation region. The lifetime of storms (at least hours) and the residence time of small particles (about 1.5 hr for a 100-μm particle) indicate that ice crystals smaller than 10 to 100μm should be entirely melted by the adsorption of NH_3 vapor.

We note that we did not consider the heat balance in the grain. Heat conduction takes place with a timescale $\tau_{\text{cond}} \sim \widetilde{d}^2 \widetilde{\rho}_{\text{H}_2\text{O}} \widetilde{c}_{P,\text{H}_2\text{O}} / \widetilde{k}_{\text{H}_2\text{O}}$ where $\widetilde{c}_{P,\text{H}_2\text{O}} \sim 1.5 \times 10^7$ erg g^{-1} K^{-1} is the heat capacity of water ice at -80°C and $\widetilde{k}_{\text{H}_2\text{O}} \sim 3.2 \times 10^5$ erg s^{-1} K^{-1} cm^{-1} its thermal conductivity. Thus, for the small grains considered, heat conduction takes place on a time scale $\tau_{\text{cond}} \sim 10^{-3}$ s, that is, extremely fast compared to the other timescales. We note however that this ignores latent heat effects, which should also be considered.

3. Growth and Transport of Mushballs

3.1. Fall Velocities

Let us first examine how particles may be lofted by updrafts or fall because of a too large mass in Jupiter's atmosphere. The terminal velocity of particles falling in the atmosphere is obtained from the equilibrium between drag force and gravitational acceleration. It is conveniently expressed as
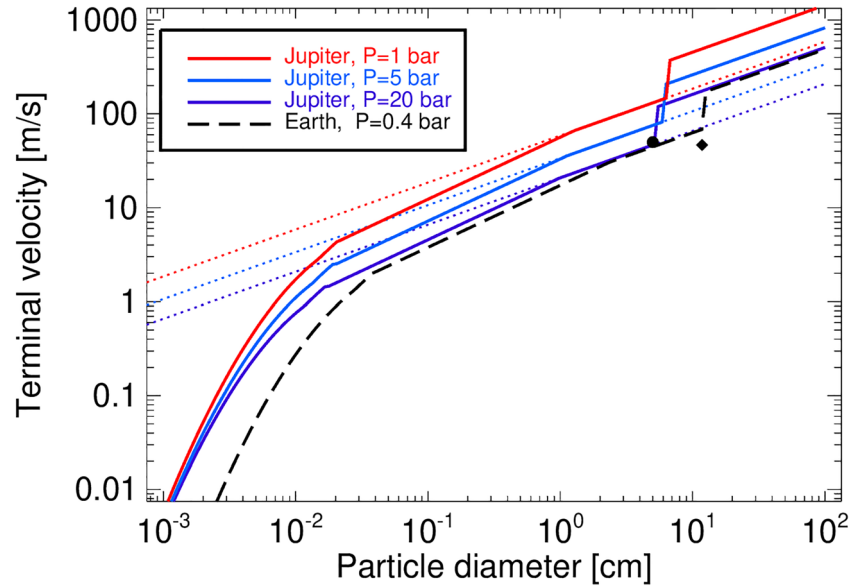
Figure 2. Terminal velocity of ice (or ammonia-ice) particles with diameters from 1μm to 1 m, for three pressure levels, 1, 5, and 20 bar inside Jupiter's atmosphere. The plain lines correspond to the full formulation. The dotted lines are the result from assuming a constant drag $C_d = 0.6$, applicable to large Earth hailstones (Rasmussen & Heymsfield, 1987). For comparison the Earth case for a pressure of 400 mbar and a temperature of −20°C is shown as a dashed line. Two examples for the Earth case are shown: The circle corresponds to 5-cm hailstones observed in a particularly powerful storm that occurred in Oklahoma on 29 May 1976, with updrafts of ∼50 m/s (Nelson, 1983). The diamond corresponds to a giant hailstone collected on 3 September 1970 also in Oklahoma, weighting 766 g, with 15.5 cm of longest dimension and 11.8 cm of effective diameter (Roos, 1972).

$$v_{\text{fall}} = \left(\frac{\frac{4}{3C_d} \widetilde{\rho} g \widetilde{d}}{\rho_a} \right)^{1/2}, \tag{2}$$

where $\widetilde{d}$ is the particle size, $\widetilde{\rho}$ its physical density, g the gravitational acceleration, ρ_a the atmospheric density and C_d is the dimensionless drag coefficient. For hard spheres, $\widetilde{d}$ is the diameter and C_d is only a function of the Reynolds number of the particle, defined as $N_{\text{Re}} = \widetilde{d} \rho_a v_{\text{fall}}/\eta_a$, with η_a being the dynamic viscosity of the atmosphere. For large spheres (mm-size or more in our case), $C_d \sim 0.47$, but in the general case, this is a function of N_{Re}, and of the shape of the particle (Pruppacher & Klett, 1997). We use the formulation of $C_d(N_{\text{Re}})$ of Rasmussen and Heymsfield (1987) based on studies of hailstones on Earth. (We correct a typo [a forgotten minus sign] in Equation (B1) of Rasmussen and Heymsfield (1987): $\log_{10} N_{\text{Re}} = -1.7095 + 1.33438W - 0.11591W^2$.)

We will see that large hailstones/mushballs in Jupiter can reach large Reynolds numbers. It is known experimentally that above a value $N_{\text{Re,crit}} \approx 3 \times 10^5$, the drag coefficient suddenly drops by a factor ∼5. While this is generally not the case on Earth for hailstones (Rasmussen & Heymsfield, 1987; Roos, 1972), it is of relevance to golf and tennis balls (Kundu & Cohen, 2016) and probably of mushballs in Jupiter. We therefore include the effect by imposing that for $N_{\text{Re}} > 3 \times 10^5$, $C_d = 0.1$. (As we will see, this level of simplification is sufficient for our purposes.)

Figure 2 shows how the terminal velocity of particles (assumed dense and spherical) varies with size at various levels in Jupiter atmosphere, and on Earth. Due to Jupiter's higher gravity and lower molecular weight of its atmosphere, terminal velocities are about four times larger than on Earth for the same pressure level.

For sizes below 100 μm, we are in the Stokes regime, implying $C_d \sim 24/N_{\text{Re}}$ and $v_{\text{fall}} \propto \widetilde{d}^2$. The fall velocities are slower than 1 m/s. At larger sizes, C_d decreases to reach a value measured to be $C_d \sim 0.6$ for real hailstones (Rasmussen & Heymsfield, 1987). At larger sizes, when reaching the critical Reynolds number $N_{\text{Re,crit}}$, the terminal velocity is expected to increase suddenly, which is represented by a kink in Figure 2. A

near-critical giant hailstone of 766 g was collected in Oklahoma and found to be slightly subcritical (Roos, 1972), with a terminal velocity measured in wind tunnels reaching 44 to 47 m/s, slightly below our theoretical curve (this can be attributed to its complex shape). On Jupiter, because of a higher kinematic viscosity, the critical Reynolds number is reached for particle sizes about three times smaller than on Earth, that is, for particle diameters above 4 to 6 cm.

We may distinguish three types of condensed particles:

- Cloud droplets and ice crystals: On Earth, most have sizes between 10 and 50 μm (Pruppacher & Klett, 1997; Rogers & Yau, 1996). Similar values are found in models of Jupiter water clouds using realistic microphysics, but with a tendency for a faster growth and thus slightly larger sizes ∼100 μm or more (Yair et al., 1995).
- Raindrops: Their maximum diameter is set by hydrodynamical stability considerations: $\widetilde{d} \sim (\gamma/\widetilde{\rho}g)^{1/2}$, where γ is surface tension and $\widetilde{\rho}$ is density of the liquid. We expect surface tension to be only weakly affected by ammonia content and temperature, implying that since on Earth the maximum droplet diameter is about 5 mm, it should be of order 3 mm on Jupiter due to its larger gravity. These maximum droplet sizes should fall with a velocity ∼20 m/s at 5 bar.
- Hailstones/mushballs: They can reach large sizes, provided that the updraft velocity balances their terminal velocity. Of course, this also requires fast growth, something that is obtained on Earth when supercooled water is present to allow an efficient sticking of droplets. The circle in Figure 2 corresponds to the maximum hailstone diameter in a powerful hailstorm that occurred in Oklahoma in 1976 and for which the maximum updraft speed was measured to be 50 m/s (Nelson, 1983). This value corresponds to the terminal velocity of these largest hailstones, showing that balance between updraft speed and terminal velocity is key. Given storms with updraft speed ranging from 10 to 100 m/s in Jupiter (Hueso et al., 2002; Stoker, 1986; Sugiyama et al., 2014), we should expect hailstones in Jupiter to be able, in principle, to reach similar sizes as on Earth.

3.2. Growth of Mushballs

We now examine how initially small (∼100 μm) water-ice crystals in a strong (∼50 m/s) updraft may adsorb ammonia, grow, collect more icy particles until they become too large to remain part of the updraft and begin to fall. Although this model is simple and may be considered naive in regard to the complexity of hail formation on Earth (Pruppacher & Klett, 1997), we believe that the framework presented here provides a useful insight into the Earth-like phenomena taking place in Jupiter's atmosphere and should help to explain Juno's observations.

The adsorption of NH_3 vapor by ice particles is expected to heterogeneous, a consequence of the temperature gradients between the core of the updraft which should be warmer by up to ∼5 K compared to the outside. The ammonia adsorption and resulting melting of the ice particles should occur faster towards the edge of updrafts because of the entrainment of this colder surrounding atmosphere.

Prior to reaching the 1.5-bar level, the growth of ice particles in the updraft could be considered as essentially stalled: larger particles having rained out, only small-size particles (between 1 and 100 μm) remain and have a low collision probability (Yair et al., 1995). Crossing the mushball-formation region suddenly has two effects: The adsorption of ammonia vapor increases particle mass by 30%. Melting also increases their density from low values (say ∼0.3g/cm³) (Davidovits et al., 2006) to that of the liquid ammonia-water mixture, that is, 0.9g/cm³. Both processes lead to an increase of the fall velocity for these particles. For example, at the 1.5-bar level, the terminal velocity of a 30-μm ice particle with a density of 0.3 g/cm³ is about 2.5 m/s; it grows to 2.7 m/s due to mass increase and to 3.9 m/s due to melting, an overall 60% increase. It is natural to assume that because of cloud heterogeneity, the differential velocities of the particles will quickly increase.

In what follows, we will use a simplified approach, by considering that, in an updraft of velocity v_{up}, one particle (hereafter "mushball") of mass $\widetilde{m}$, diameter $\widetilde{d}$, and terminal velocity v_{fall} grows at the expense of other particles (hereafter "cloud droplets") with comparatively much smaller terminal velocities. The mass of the mushball, its altitude z, and ammonia mixing ratio evolve with time according to the following relations:

$$\frac{d\widetilde{M}_{H_2O}}{dt} = E\frac{\pi}{4}\widetilde{d}^2\mu_{H_2O}\widetilde{x}_{H_2O}\frac{P}{\mathscr{R}T}v_{fall},$$ (3)

$$\frac{d\widetilde{M}_{N}H3}{dt} = E\frac{\pi}{4}\widetilde{d}^2\mu_{NH_3}\widetilde{x}_{NH_3}\frac{P}{\mathscr{R}T}v_{fall},$$ (4)

$$\frac{dz}{dt} = v_{up} - v_{fall},$$ (5)

where $\widetilde{M}_{H_2O}$ and $\widetilde{M}_{NH_3}$ are the mushball masses in water and ammonia, respectively, μ_{H_2O} and μ_{NH_3} the molecular masses, $\widetilde{x}_{H_2O}$ and $\widetilde{x}_{NH_3}$ their volume mixing ratios in the condensed phase (as cloud droplets), and E is the collection efficiency. Since we assume sphericity mass and diameter are related by $\widetilde{M} = \widetilde{M}_{H_2O+\widetilde{M}_{NH_3}} = (\pi/6)\widetilde{\rho}\widetilde{d}^3$ where $\widetilde{\rho}$ is the physical density of the mushball.

The value of $\widetilde{x}_{H_2O}$, the mixing ratio of condensed water, is set by the ability of the storm to loft small icy particles to the region considered. Because at the temperatures that we consider, the vapor pressure of water is extremely low (see Figure 1), we assume that $\widetilde{x}_{H_2O} = x_{H_2O}$, the total mixing ratio of water. Yair et al. (1995) find a mass mixing ratio of water at the 1 bar level that can reach 1 g/kg, corresponding to $\widetilde{x}_{H_2O} = 133$ ppmv. This value is obtained for a solar-composition atmosphere and should increase for a higher deep abundance of water. We also note that higher values are likely due to a feedback mechanism not considered in that study: The formation of mushballs can increase updraft speed by decreasing condensate load at depth and by creating strong horizontal temperature gradients upon melting and evaporation. On the other hand, cloud-ensemble simulations (Sugiyama et al., 2014) using the so-called Kessler parameterization of microphysical processes (Kessler, 1969) impose a conversion rate from nonprecipitating condensates to precipitating condensates that cannot be used to reliably predict the amount of small-size particles at high altitudes. We thus adopt three possible values of $\widetilde{x}_{H_2O}$, 100, 600, and 1,200 ppmv.

The value of $\widetilde{x}_{NH_3}$, the mixing ratio of condensed ammonia, is set by the abundance of ammonia vapor x_{NH_3}, the value of $\widetilde{x}_{H_2O}$ and the location in the phase diagram set by the pressure and temperature conditions. We consider that $\widetilde{x}_{NH_3} = 0$ in the pure H_2O ice region of the phase diagram. Mushballs start forming when liquid $H_2O \cdot NH_3$ forms, at pressures $P \lesssim 1.5$ bar and temperatures $T \lesssim 188$ K for $x_{NH_3} = 360$ ppmv, corresponding to the global ammonia abundance of the north Equatorial Zone (Li et al., 2017). In order to calculate $\widetilde{x}_{NH_3}$, we determine for the temperature of the levels considered the intersections with the pure H_2O ice phase and with the $H_2O \cdot NH_3$ ice phase. We derive the corresponding values of the ammonia vapor mixing ratio, x_1 and x_2, respectively. If $x_1 < x_{NH_3} \leq x_2$, the equilibrium is between $H_2O \cdot NH_3$ liquid and H_2O ice. If $x_2 < x_{NH_3}$, at temperatures $T \lesssim 170K$, it is between $H_2O \cdot NH_3$ ice, $H_2O \cdot NH_3$ liquid, and H_2O ice. By assuming full thermodynamic equilibrium and that $H_2O \cdot NH_3$ liquid contains 2/3 H_2O and 1/3 NH_3, we derive

$$\widetilde{x}_{NH_3} = \begin{cases} 0 & \text{if } x_{NH_3} \leq x_1, \\ \min\left[x_{NH_3} - x_1, \widetilde{x}_{H_2O}/2\right] & \text{if } x_1 < x_{NH_3} \leq x_2. \\ \min\left[x_{NH_3} - x_1, \widetilde{x}_{H_2O} + (x_{NH_3} - x_2)/2, \widetilde{x}_{H_2O}\right] & \text{if } x_{NH_3} > x_2. \end{cases}$$ (6)

Based on the values of $\widetilde{M}_{H_2O}$ and $\widetilde{M}_{NH_3}$, we can calculate the mass fraction of ammonia in the mushballs

$$\widetilde{f}_{NH_3} = \frac{\widetilde{M}_{NH_3}}{\widetilde{M}_{NH_3} + \widetilde{M}_{H_2O}}.$$ (7)

Conversely, the mass fraction of water is $\widetilde{f}_{H_2O} = 1 - \widetilde{f}_{NH_3}$.

The collection efficiency depends on (1) how ice particles follow the flow around the mushball and (2) how effectively they remain bound upon collision. The first parameter is directly linked to the Stokes parameter

of the ice particles, that is, the ratio of their stopping time to the mushball-crossing time $v_{\text{fall}}/\tilde{d}$. For the ice particles that we consider, we are in the Stokes regime, implying a Stokes number $St \sim \tilde{\rho}_{\text{particle}}\tilde{s}_{\text{particle}}^2 v_{\text{fall}}/(18\eta_a d)$, where $\tilde{\rho}_{\text{particle}}$ and $\tilde{s}_{\text{particle}}$ are the particle physical density and size, respectively (Kundu & Cohen, 2016). For $\tilde{\rho}_{\text{particle}} = 0.3$ g cm^{-3} and $\tilde{s}_{\text{particle}} = 100$ μm, and using the approximation that $C_d = 0.6$ for mushballs in the 0.1- to 5-cm size range, we obtain $St \sim 100(\tilde{d}/1\text{ cm})^{1/2}$ implying that hydrodynamic effects should not decrease the collection efficiency (Homann et al., 2016).

Altogether, the collection efficiency E, is difficult to estimate. In the Earth's atmosphere, its value for collisions between ice particles ranges between unity to less than 0.1 (Phillips et al., 2015). Being at or close to the melting temperature is a key feature of the ability of particles to stick. Extrapolating these results to the Jupiter case, we thus expect $E\sim1$ when thermodynamic conditions predict the presence of liquid $NH_3 \cdot H_2O$ and a smaller value away from that regime. For simplicity, we assume that $E = 0.3$ in the regime where the only condensates are made of H_2O ice and $E = 1$ elsewhere, but also explore other possibilities.

3.3. Evaporation of Mushballs

As mushballs fall into a high-enough temperature region, they will begin to melt and evaporate. In order to account for this process, we use the approach derived for the melting of hail on Earth (Pruppacher & Klett, 1997). The rate at which hail melts is controlled by heat conduction from the atmosphere into the hailstone, the development of an interface between liquid water and solid ice inside the hail stone and the shedding of the water shell due to hydrodynamic instabilities. The hailstone is kept cooler than the surrounding atmosphere due to latent heat release by evaporation.

The evolution of the hailstone structure upon melting can be relatively complex: A water torus generally forms and shedding of either small or large drops can take place. Depending on the hailstone size, this can take place either continuously or intermittently. At millimeter sizes, an eccentric melting of the ice core takes place (Rasmussen et al., 1984).

Here, we use a simplified approach that considers that shedding takes place instantaneously. In that case, the hailstone is kept near its melting temperature $\tilde{T}_0 \sim 0°C$ and its size is governed by the following equation (Pruppacher & Klett, 1997):

$$\frac{da}{dt} = \frac{1}{\left(L_m + \tilde{c}_{P,H_2O}\Delta\tilde{T}\right)\rho_i a}\left[-k_a\left(T - \tilde{T}_0\right)f_h + D_{H_2O}\frac{\mu_v L_v}{\mathscr{R}}\left(\frac{P_{\text{sat}}\left(\tilde{T}_0\right)}{\tilde{T}_0} - H_a\frac{P_{\text{sat}}(T)}{T}\right)f_v\right], \quad (8)$$

where f_h and f_v are ventilation coefficients for heat and vapor, respectively, and are measured experimentally to be

$$\begin{aligned} f_h &= \frac{\chi}{2}N_{\text{Re}}^{1/2}\left(\frac{\nu_a}{K_a}\right)^{1/3}, \\ f_v &= \frac{\chi}{2}N_{\text{Re}}^{1/2}\left(\frac{\nu_a}{D_{H_2O}}\right)^{1/3}. \end{aligned} \quad (9)$$

The following quantities have been used: L_m and L_v are the latent heat of melting and vaporization, respectively (accounting for their temperature dependence, but assuming pure H_2O), k_a is the thermal conductivity of the atmosphere, ν_a its kinematic viscosity, $K_a = k_a/(\rho c_P)$ its thermal diffusivity, D_{H_2O} the diffusivity of water vapor in the atmosphere, P_{sat} the saturation pressure, H_a the relative humidity of the atmosphere, N_{Re} is the Reynolds number defined in the terminal velocity section, and χ is a mass transfer coefficient of order unity. Given the extended fall, we account for the internal temperature change of the hailstone, with $\tilde{c}_{P,H_2O}$ being the specific heat and $\Delta\tilde{T} = \tilde{T}_i - \tilde{T}_0$ the difference between an internal temperature $\tilde{T}_i$ and that at the surface $\tilde{T}_0$.

Given the large Reynolds number (10^3 to 10^6) considered here, the ventilation coefficients are large and represent the largest effect governing the melting of the hailstone. The Prandtl and Schmidt numbers that enter these coefficients are close to unity: As seen from Table B1, $(\nu_a/K_a)^{1/3}\sim0.88$ and $(\nu_a/D_{H_2O})^{1/3} \sim 1.05$

so that to first approximation $f_h \sim f_v$. Experiments suggest that $\chi \sim 0.76$ (Pruppacher & Klett, 1997). Overall, this yields $f_h \sim f_v \sim$ 10 to 400. We note that this scaling law should change in the supercritical regime ($N_{Re} \gtrsim 3 \times 10^5$), but it is not even clear whether melting should be increased or decreased over this relation. Dedicated experiments should be conducted in order to determine more precisely the mushball evaporation level.

Although most of the complex processes observed during hailstone melting are not included, Appendix A.1 shows that the approach does reproduce relatively well observations in the Earths atmosphere and in wind tunnels. It also shows that additional heating due to viscous drag can be neglected.

3.4. The Rise and Fall of Mushballs in Jupiter's Atmosphere

We now apply our model for growth and evaporation of mushballs to the case of Jupiter. We are interested in situations where storms are able to reach the upper regions of the atmosphere (above the 1 bar pressure level). This corresponds to large storms. We thus assume an updraft velocity of 50 m/s generated from the cloud-base level and extending to the 0.4-bar level (Hueso et al., 2002; Sugiyama et al., 2014). We assume that the upward velocity goes to zero away from that pressure range gradually with an error function:

$$v_{up} = v_0 \left\{ 1 - \mathrm{erf} \left[\max \left(0, -\frac{\log_{10}(P/P_{top})}{\delta_P} \right) \right] \right\} \left\{ 1 - \mathrm{erf} \left[\max \left(0, \frac{\log_{10}(P/P_{bottom})}{\delta_P} \right) \right] \right\}, \qquad (10)$$

and we choose $P_{top} = 0.4\,\mathrm{bar}$, $P_{bottom} = 5$ bar and $\delta_P = 0.05$. (The precise values are not important, as long as the updraft takes place at pressures between say, 0.5 and 1.5 bar.)

Based on terrestrial data showing that graupels and ice crystals have densities ranging from 0.05 to 0.9 g/cm^3 (Pruppacher & Klett, 1997), we adopt a physical density both for H_2O ice and for $H_2O \cdot NH_3$ ice of 0.3 g/cm^3. In the region where $H_2O \cdot NH_3$ liquid forms, we assume that the collected ice have a density of 0.9 g/cm^3. In that region, we also assume that the mushball melts partially to an overall density of 0.9 g/cm^3.

We use the following values of the physical parameters, evaluated at 300 K, which corresponds approximately to the atmospheric temperature where mushballs melt: for water ice, $c_P = 2.0 \times 10^7\,\mathrm{erg\ g^{-1}\ K^{-1}}$, $L_m = 3.34 \times 10^9\mathrm{erg\ g^{-1}}$; for water vapor, $L_v = 2.515 \times 10^{10}\mathrm{erg\ g^{-1}}$, $D_{H_2O} = 0.17\mathrm{cm^2\ s^{-1}}$, $\mu_v = 18$; for hydrogen, $k_a = 1.85 \times 10^4\mathrm{erg\ s^{-1}\ cm^{-1}\ K^{-1}}$. We further assume that $H_a = 1$, except below the cloud base, assumed to be at 5.8 bar, corresponding to an enrichment of water equal to 2.7 times the protosolar value (Li et al., 2020). (As shown in Appendix A.3, this assumption has negligible consequences for the outcome of the model.)

We use a temperature profile that is based on the Galileo probe measurements (Seiff et al., 1998) and extended below 22 bars using an adiabatic profile derived from an interior model of Jupiter (Guillot et al., 2018).

Figure 3 shows the resulting evolution of mushballs for three cases: Global abundances of water ice carried above the 1-bar level of 100, 600, and 1,200 ppmv, respectively. The simulation starts when water-ice particles generated at depth by the storm and carried in the updraft reach the 1.5-bar level. We start from an initial seed of 100 μm that melts due to NH_3 adsorption, starts collecting $H_2O \cdot NH_3$ liquid and, for the 600 and 1,200 ppmv water-ice cases, H_2O ice particles. Its terminal velocity is small compared to the updraft velocity. When reaching the 1-bar region, the particle accretes solid $H_2O \cdot NH_3$ and H_2O ice. It continues to ascend until it has grown to a point where its terminal velocity equals the updraft velocity. At this point, it will start to fall, scavenging more particles on the way.

Between 1.1 and 1.5 bar, the mushball crosses again the liquid $H_2O \cdot NH_3$ region and partially melts. The density change (to about $\sim 0.9\ \mathrm{g\ cm^{-3}}$) yields an increase of the Reynolds number. For the middle and high ice abundance case, it becomes supercritical, which yields a very significant increase of the terminal velocity to about 300 m/s. (In the low-abundance case, the density change is not sufficient and the velocity stays confined to ~ 100 m/s.)

In this same range of pressures, the scavenging of H_2O ice leads to a progressive increase of the H_2O mass in the mushball. The fraction of NH_3 decreases to a minimum of 3% in the high water-ice case to 20% in the low water-ice case. At that point, the temperature has reached 0°C, the water-ice melting point, which leads to a progressive melting of the outer shell of the mushball. The NH_3 fraction thus increases up to the value it had
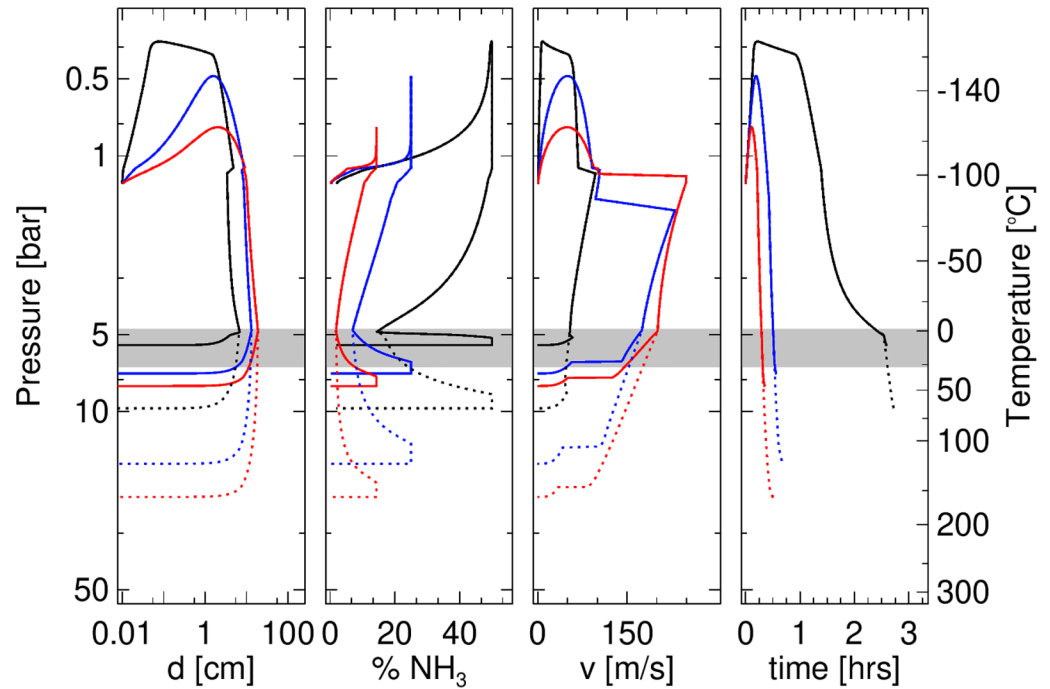
Figure 3. Characteristics of hail/mushballs as a function of pressure in Jupiter, for three values of the abundance of water-ice particles in the upper atmosphere: 100 ppmv (black), 600 ppmv (blue), and 1,200 ppmv (red), assuming an updraft velocity of 50 m/s (see text). The first panel shows the diameter of hailstones, the second one the percentage of NH_3 molecules that they contain, the third one their terminal velocity and the fourth one the time spent since their formation. The dotted lines correspond to cases in which the ventilation factor has been decreased by a factor 10 compared to the nominal value (see text). The temperatures in Jupiter's atmosphere are indicated on the right. The gray area corresponds to the location of the water cloud base, that is, between 4.8 and 6.7 bar according to the Juno measurements (Li et al., 2020).

after crossing the liquid $H_2O \cdot NH_3$ region. The last phase is a very quick melting and evaporation of the mushball, at pressures of 6.3, 8.1, and 9.6 bar for the low, medium, and high water-ice cases, respectively. If we decrease the ventilation factor by an order of magnitude (to account for possible changes of the empirical relation at high Reynolds number), the mushballs penetrate deeper, that is, to 10, 17, and 24 bar, respectively (see Figure 3).

We find the depth at which mushballs evaporate to be insensitive to our choice of the drag coefficient C_d for supercritical Reynolds numbers due to a balance between shorter timescales and larger ventilation coefficients. However, the time taken for mushballs to reach the evaporation level is proportional to $\sqrt{C_d}$ and is thus correspondingly shorter due to the supercritical Reynolds number effect.

We can derive several important conclusions from this relatively simple model: The first one is that during strong storms, ammonia can be efficiently carried from the top of Jupiter's atmosphere down to levels below the water-cloud base. This is the case at least for the medium and high water-ice abundances. Equally significantly, for a number of cases, NH_3 is carried below the water cloud base more efficiently than H_2O, that is, $\widetilde{f}_{NH_3}/\widetilde{f}_{H_2O} > (N/O)_\odot = 0.135$, or equivalently $\widetilde{f}_{NH_3} > 0.117$, where $(N/O)_\odot$ is the protosolar nitrogen to oxygen mixing ratio (Lodders, 2003). This implies that the downward transport of ammonia by water storms is efficient and can lead to a depletion of the upper atmosphere ammonia.

An exploration of the sensitivity to the parameters of the model is presented in Appendix A.3. The depth of penetration of mushballs extends from 5.1 to 31 bar, depending on parameter values (quantity of water ice, updraft velocity, sticking efficiency, etc.). The cases for which water ice evaporate mostly above the water cloud base and the mushball core is deposited below appear most favorable. In that case, evaporated water may be recycled into storms while the aqueous ammonia mixture at the core of the mushballs would then be able to form evaporative downdrafts below the cloud base. Storms with updraft velocities between 10 and 50

Phase	Morphology	Size	Pressure	Comments
0	·	10-100μm	4.5-1.1 bar	H_2O ice crystal
1	●	100μm-1mm	1.5-1.1 bar	$H_2O \cdot NH_3$ liquid + H_2O ice slush
2	✦	1mm-5cm	1.1-0.5 bar	$H_2O \cdot NH_3$ liquid core surrounded by shell of low density $H_2O \cdot NH_3$ ice and H_2O ice
3	✦	2-3cm	1.1-1.5 bar	$H_2O \cdot NH_3$ liquid core surrounded by H_2O ice shell
4	✦	3-10cm	1.5-5 bar	$H_2O \cdot NH_3$ liquid core surrounded by H_2O ice shell (possibly porous away from the core)
5	◉	10-2cm	5-10 bar	$H_2O \cdot NH_3$ liquid core H_2O ice crust H_2O water shell
6	●	2-0cm	7-11 bar	Evaporating $H_2O \cdot NH_3$ liquid droplet

Figure 4. The phases and internal structure of mushballs.

m/s and between 100 and 600 ppmv of water ice carried to the 1.5 bar region therefore seem most promising to account for the Juno data.

Of course, we must add several important caveats. Compared to models of hail formation on Earth, this one is extremely simplified. In particular, it does not include complex geometrical effects inherent to hailstorm formation on Earth, the effect of turbulence within the cloud, the combined growth of a population of particles, and feedbacks due to evaporative cooling. On the other hand, it does show that a simple model can already account for the formation of ~10-cm mushball hail in Jupiter. When putting Earth and Jupiter in perspective, we note that Earth can form large hailstones (up to 0.77 kg; see, e.g., Roos, 1972), that this requires strong updrafts (~50 m/s) and the presence of liquid water droplets that are supercooled to around −15°C (Pruppacher & Klett, 1997), a relatively rare occurrence. Jupiter has equivalently strong updrafts (Hueso et al., 2002; Gierasch et al., 2000; Stoker, 1986; Sugiyama et al., 2014), and the presence of a liquid phase in contact with solids is guaranteed as long as ice particles are carried at least to the 1.5-bar level (which occurs only for storms with already large upward velocities). Two important differences are that on Jupiter large storms (characterized by large updraft velocities >10 m/s at 2 bars) should always be able to loft ice particles to the 1.1- to 1.5-bar region where melting occurs, that the range of altitudes over which growth by scavenging can take place is vastly larger (~50 km in Jupiter versus ~3 km on Earth). This points to a hail formation mechanism on Jupiter that should be significantly more efficient than on Earth.

3.5. Internal Evolution of Mushballs

Figure 4 examines the evolution of the internal structure of the mushballs. We identify six evolution phases:

- Phase 1: Early adsorption of NH_3 into an H_2O ice crystal, its melting and subsequent growth. For high enough abundances of H_2O ice, the melting should be partial; that is, a relatively high-density slush should form.
- Phase 2: Growth by accretion of low-temperature, porous ices ($H_2O \cdot NH_3$ and H_2O).

- Phase 3: Partial melting of the mushball with continuous accretion of H_2O ice.
- Phase 4: Accretion of low-density H_2O ice crystals.
- Phase 5: Melting of the outer H_2O shell and shedding. The size and mass decrease.
- Phase 6: Evaporation of the $H_2O\cdot NH_3$ core.

The buildup of an H_2O ice shell in Phase 3 is critical because it isolates the liquid core of the mushball thermally and prevents NH_3 from diffusing out and be lost to the atmosphere. Even though the ice crystals collected should be very porous, the part of the H_2O ice shell in contact with the $H_2O\cdot NH_3$ liquid is expected to be compact due to its interaction with the liquid.

Thermal equilibration within the mushball takes place with a characteristic time of order $\tau \approx d^2/\alpha_i$ where $\alpha_i \sim 2.2 \times 10^{-2}\,cm^2\,s^{-1}$ is the thermal diffusivity of H_2O ice. It is thus approximately only 45 s for a 1-cm mushball but 1.3 hr for a 10-cm one. For comparison, the examples shown in Figure 3 correspond to fall-times of ~ 40 min from 1.5 to 5 bar for the 100-ppmv H_2O abundance case and only about 5 min from 1.5 to about 10 bar for the two other cases. Thermal equilibration will lead to a progressive melting of the H_2O ice crust of the mushball from the inside-out and a decrease of the ammonia concentration in the mushball core. It could lead to a sudden break-up of the mushball when the H_2O crust becomes too thin. This effect should be examined but should not affect our conclusions qualitatively.

Similarly, diffusion of ammonia through the solid-ice crust is expected to be slow. The diffusion coefficient for ammonia in water ice measured experimentally at 142 K is $\widetilde{D}_{NH_3}^{sol} \sim 4 \times 10^{-10}\,cm^2/s$ (Livingston et al., 2002). This may be extrapolated to be up to two orders of magnitude higher at ~ 250 K, based on Na which has a similar behavior (Livingston et al., 2002). Thus, using the same approach as in section 2.2, we expect ammonia to diffuse outward only by about $\sim 100\,\mu m$ in 1 hr, that is, a negligible amount given that we expect approximately centimeter sizes for the mushballs.

Importantly, the highly concentrated ammonia-water mush at the center would be delivered last in Jupiter's deep atmosphere. Some of the water that is evaporated at higher levels can thus be recycled to power new storms and lead to the formation of more mushballs.

4. Importance of Evaporative Downdrafts

For our nominal ventilation coefficient, the evaporation of mushballs occurs near 10 bars, a pressure level that is not sufficiently deep to account for abundance increase inferred from the Juno MWR data (Bolton et al., 2017; Li et al., 2017). One possibility is that ventilation coefficients in the supercritical regime are decreased. However, an other mechanism, the presence of evaporative downdrafts, must lead to further sinking of ammonia (and water).

On Earth, any rain, snow, or hail accumulates on the surface. In Jupiter, the absence of such a surface implies that a pocket of gas with an increased concentration of ammonia and water must form. It is difficult to estimate precisely the concentration increase because it depends on geometrical factors and the time evolution of the storm. But we estimate that it may be substantial. Let us assume a storm surface area σ_{storm}, an updraft velocity v_{up} for a typical characteristic timescale Δt. The mushballs evaporate lower than the cloud base, in an area σ_{down} and down on to a depth H_{down}. The typical densities are $\rho_{storm} \sim 5 \times 10^{-4}\,g\,cm^{-3}$ around 5 bar and $\rho_{down} \sim 2 \times 10^{-3}\,g/cm^3$ around 30 bar. The enrichment (i.e., fractional increase of the mixing ratio of water and ammonia) is of order $\Delta x \sim \epsilon x (\sigma_{storm}/\sigma_{down})(\rho_{storm}/\rho_{down})(v_{up}\Delta t/H_{down})$. The first term in parenthesis is of order unity; the second one is $\sim 1/6$. The Voyager storm analyzed by Hueso et al. (2002) took about 10 days to develop and seemed relatively well fixed in latitude and longitude (on the local differential rotation frame). We hence estimate that $H_{down} \sim 100$ km, $v_{up} \sim 50$ m/s, and $\Delta t \sim 3$ hr. The last term in parenthesis is thus $v_{up}\Delta t/H_{down} \sim 5$. With an assumed mushball formation rate $\epsilon \sim 0.3$, we thus get $\Delta x/x \sim 0.25$. This is of course only an order of magnitude estimate and could vary significantly depending on the storm geometry and velocity. It is likely that localized bubbles that are highly enriched in water and ammonia will form and be only weakly affected by turbulence, thus effectively increasing Δx much above that value.

In fact, even a modest enrichment can power strong downdrafts: For a perfect gas with a volume mixing ratio of vapor x, with $\zeta = \mu_v/\mu_d$ being the ratio of the mean molecular mass of vapor to that of dry gas

$$\rho = [1 + (\zeta - 1)x]\frac{\mu_d P}{\mathscr{R}T}. \tag{11}$$

Evaporation of water (and ammonia) will result in an increase of mean molecular weight (due to the addition of vapor) and a cooling by evaporation, leading to a density increase

$$\frac{\Delta\rho}{\rho} \approx (\zeta - 1)\Delta x - \frac{\Delta T}{T}, \tag{12}$$

where we assumed $x \ll 1$. The change in temperature due to evaporation is $\Delta T = L_v \zeta \Delta x / c_P$, where L_v is the latent heat of vaporization per unit mass of condensate (water) and c_P is the heat capacity per unit mass of atmosphere. Thus, we can rewrite the density change as a function of the increase in vapor mixing ratio

$$\frac{\Delta\rho}{\rho} \approx \left(\zeta - 1 + \frac{L_v \zeta}{c_P T}\right)\Delta x. \tag{13}$$

For our conditions, we get $\zeta - 1 \approx 6.8$ and $L_v \zeta / c_P T \approx 4.7$; that is, the increase in mean molecular weight dominates slightly over the effect of evaporating cooling.

An estimate of the downdraft velocity can be obtained by calculating the work of the buoyancy force over a depth ℓ and by equating half of this work to the kinetic energy. This implies

$$v_{down} \approx \left(g\frac{\Delta\rho}{\rho}\ell\right)^{1/2}. \tag{14}$$

For a length equal to the pressure scale height $\ell \sim H_P \sim 30$ km, and Jupiter's gravity, we get $v_{down} \approx 100(\Delta x/10^{-3})^{1/2}$ m/s. For comparison, Sugiyama et al. (2014) obtain downdrafts reaching about 50 m/s. We point out that downdrafts have been recognized to be an essential part of the Sun's convection (Stein & Nordlund, 1998). In Jupiter, downdrafts are powered both by evaporative cooling and by molecular weight effects and should play an even more prominent role (Ingersoll et al., 2017).

Figure 5 illustrates what might be occurring in Jupiter with a simple experiment. Milk and water are fully miscible, like ammonia and water with hydrogen below the water cloud base in Jupiter. But when adding a spoonful of milk in the glass of water, instead of slowly diffusing in the glass, it rapidly sinks to the bottom through "milk plumes." These result from Rayleigh-Taylor instabilities, which are of course well known in hydrodynamics (see, e.g., Turner, 1969). Here, our purpose is to illustrate the fact that this process, while of minor importance in the Earth atmosphere (moist air is slightly lighter than dry air at the same temperature), is likely to play a crucial role in Jupiter. (Of course, our water and milk experiment is strongly affected by wall effects and cannot be used to infer the depth of the plumes. In Jupiter, compression effects, turbulence, and horizontal mixing are factors that should all be taken into account to infer the possible vertical extent of these downdrafts.) Unfortunately, its modeling and proper inclusion into global atmospheric models is notoriously difficult because of the variety of scales involved.

We also note that collective effects may play a role in leading to a further sinking of the condensates (water and ammonia) in Jupiter: In mushball regions, the temperatures should be locally cooler by $\delta T/T \approx -4.7\Delta x$. We have estimated for the whole column that $\Delta x \approx 0.25x$, that is, a quantity of order 10^{-3}. But it is likely that in some regions, this value is much larger than that, in which case the evaporation would be delayed by the low temperature of the downwelling plume. For example, if $\Delta x \sim 10^{-2}$, at the 10 bar pressure level where the temperature should be 65°C, it would be locally depressed to 50°C, corresponding to an increased sinking by ~ 8 km. Furthermore, the formation of a downdraft also means a faster downward transport of the mushballs with delayed evaporation. Detailed hydrodynamical simulations should be conducted in order to estimate the depth to which ammonia- and water-rich bubbles can be transported to.

Last but not least, we note that for the sinking to stop, the surrounding vapor mixing ratio must increase with depth so that the buoyancy force reverses. The location and magnitude of this increase will depend on local turbulence, entrainment of gas both in updrafts and downdrafts, on the radiative cooling of the plumes and
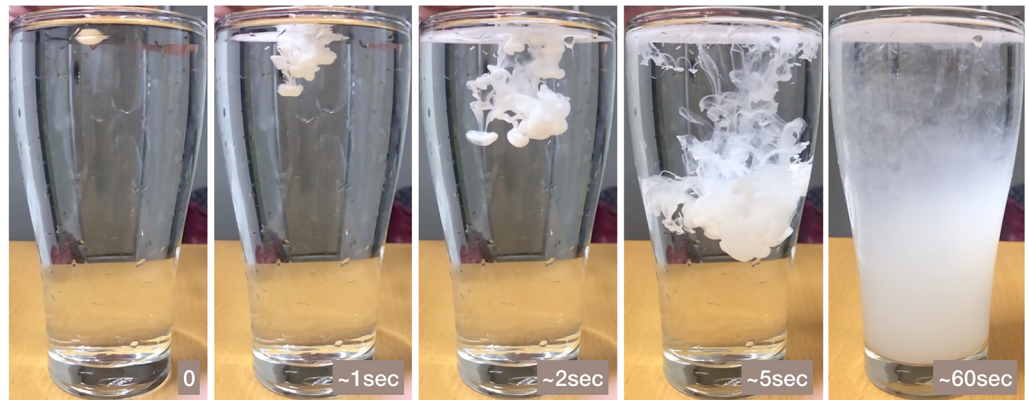
Figure 5. Simple experiment to illustrate the importance of localized downdrafts in fluid mixtures. Here, at $t = 0$, a tea spoon of fat milk from the refrigerator (~10°C) is added to a glass of water at room temperature (~20°C). Although the milk would be able to dissolve homogeneously in the glass, its slightly higher density resulting from its higher mean molecular weight and lower temperature yields strongly localized downdrafts. The final state is characterized by a gradient of increasing milk concentration with depth. Similarly, we expect strong storms in Jupiter to deliver to about 10 bar a cold and relatively highly concentrated water- and ammonia-rich gas leading to downdrafts able to reach the deeper levels of the planets. Individual storms should have horizontal extents of about ~25 km (Hueso et al., 2002) and Juno measurements indicate that ammonia concentration increases on a vertical scale of at least 100 km. Although this is largely coincidental, we note that the geometry for that simple experiment is relatively similar to that in Jupiter.

on global horizontal mixing. This problem is beyond the scope of the present work, but it is likely to have deep consequences for our understanding of the interior structure of the planet.

5. Conclusion

The variability of ammonia's concentration as a function of latitude and to great depths in Jupiter's deep atmosphere (Bolton et al., 2017; Li et al., 2017) is one of the most important surprises of the Juno mission and remains thus far unaccounted for. We have shown that thermoequilibrium chemical calculations predict the existence of a low-temperature region in which ammonia and water can form a liquid mixture with a high (~1/3) concentration of ammonia. This region is located between 1.1 and 1.5 bar and temperatures between 173 and 188 K. Jupiter's powerful storms can deliver water-ice crystals to that region. We have shown that ammonia vapor can dissolve into the ice crystals to form a high viscosity liquid ammonia-water "mush," on timescales of minutes to tens of minutes. The increased mass and density of the particles thus formed increases differential velocities and the presence of liquid is expected to also lead to a high sticking efficiency, two factors that are crucial for the growth of hail-like particles that we call "mushballs." We have presented a simple model to account for their growth, their fall to the deep atmosphere and their evaporation. Depending on the amount of water-ice particles lofted by the storms, and depending on the poorly known ventilation coefficients governing heat conduction efficiency from the atmosphere to the mushballs, they should reach pressure levels of 5 bars and even as deep as 27 bars. Further sinking is warranted by the fact that the evaporated mushballs both have a high molecular weight and low temperature.

The fact that the cores of the mushballs contain a mixture that is highly concentrated in ammonia and the fact that this core is the last to be evaporated provides a potential mechanism to explain the ammonia depletion in a large fraction of Jupiter's atmosphere. Their evaporation deeper than the water cloud level and their further transport by downdrafts can potentially explain the great depth to which ammonia depletion is observed by Juno. We note (i) that since ammonia is at the center of the mushballs, it is delivered last, (ii) that H_2O that evaporated on the way can be reused in other thunderstorms and therefore cycles further ammonia depletion, (iii) that the NH_3/H_2O concentration at the center of mushballs is ~0.3, much greater than the solar N/O ratio of 0.1320, implying that the mechanism is efficient. We also note that the minimum in the derived NH_3 abundances (Bolton et al., 2017; Li et al., 2017) is very close to the minimum NH_3 abundance below which the mushball mechanism cannot work (i.e., from Figure 1, a partial pressure

$P_{\mathrm{NH_3}} \sim 10^{-4}$ bar, corresponding to a $\sim$100 ppmv $\mathrm{NH_3}$ mole fraction in Jupiter). Finally, recent Juno observations in the optical show lightning flashes that are formed between 1 and 2 bar, consistent with the presence of liquid $\mathrm{NH_3 \cdot H_2O}$ and large particles in the mushball formation region (Becker et al., 2020). In a subsequent paper, we develop a model of Jupiter's deep atmosphere to attempt to reproduce the dominant features of Juno's observations.

Appendix A: Evaporation of Hail

A.1 Application to the Earth Case

We apply our simple model for the evaporation of hailstones and mushballs (Equations 8 and 9) to the case of the Earth atmosphere, based on the work of Rasmussen and Heymsfield (1987). We assume the Earth gravity, $g = 981$ cm/s^2, and extremely simplified model reproducing the case of Rasmussen and Heymsfield (1987), from altitude $z = 0.8$ km to $z = 5.2$ km, pressure from 0.9 to 0.6 bar, temperature from 24°C to 0°C and a relative humidity between 60% to 100% at the highest altitude where the hail originates. The mean molar weight of air is $\mu = 29$, its thermal conductivity $k_a = 2570$ erg s^{-1} cm^{-1} K^{-1}, its dynamic viscosity $\eta = 1.8 \times 10^{-4}$g cm^{-1}s^{-1} and the diffusivity of water in air, 0.3cm^2/s. The other parameters are the same as for Jupiter.

Figure A1 compares observational data and theoretical tracks (Rasmussen & Heymsfield, 1987) to results of our model calculated with Equations 8 and 9. Some differences are visible, but they are small compared to other uncertainties in the model.

A.2 Effect of Drag Heating

In the case of Jupiter, the high fall speed of mushballs raises the question of whether drag friction (not included in Equation 8) may lead to an even faster evaporation. This can be estimated as follows: Assuming an approximate constant terminal velocity, the energy dissipated per time Δt by drag is $\Delta E \sim \widetilde{M} g\, v_{\mathrm{fall}} \Delta t$. Because the size considered is much smaller than the mean free path, this energy is dissipated in the gas and can then potentially heat the mushball. The part that is of interest to us is the fraction ϵ_{drag} that is dissipated in the boundary layer around the mushball, which has a thickness $\ell \sim \sqrt{K_a d / v_{\mathrm{fall}}}$. With $K_a \sim 0.3$
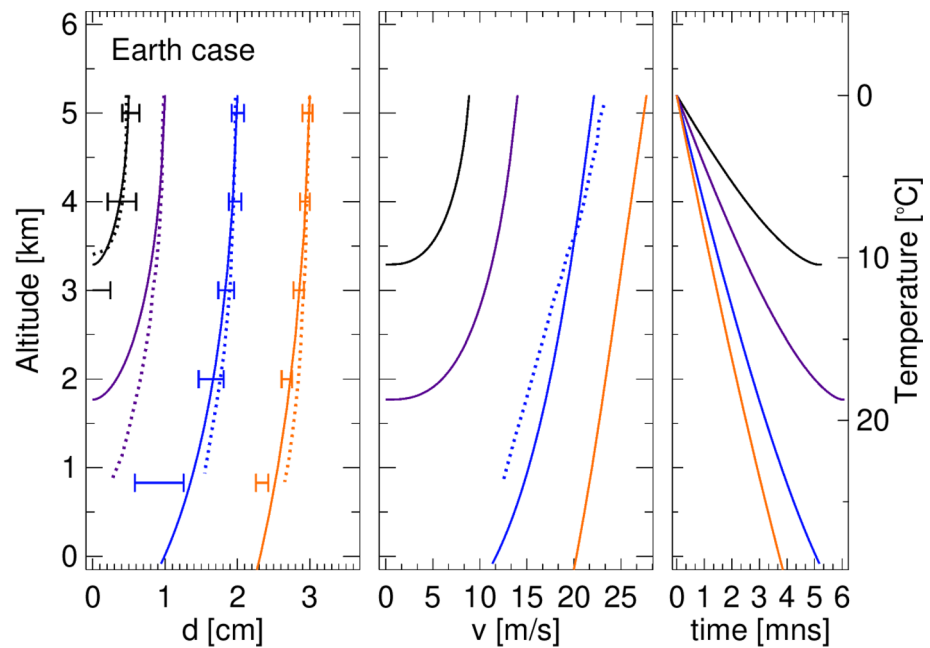
Figure A1. Comparison of the evolution of hailstones obtained from wind tunnel experiments (horizontal error bars), dedicated calculations (Rasmussen & Heymsfield, 1987) (dotted curves) and our simple model (plain lines). The three panels show the evolution with altitude of the hailstone diameter (left), terminal velocity (center), and time (right). The colored lines correspond to different initial diameters: 0.5 cm (black), 1 cm (purple), 2 cm (blue), and 3 cm (orange).

cm^2/s, $d \sim 10$ cm and $v_{\text{fall}} \sim 300$ m/s, we obtain $\ell \sim 0.01$ cm. The gas in the boundary layer of volume $V \sim \pi d^2 \ell$ is replaced at a rate $\Delta t \sim d/v_{\text{fall}}$, implying a change of temperature in the gas

$$\Delta T \sim \epsilon_{\text{drag}} \frac{\Delta E}{c_{P,a} \rho_a V} \sim \epsilon_{\text{drag}} \frac{1}{6} \frac{\widetilde{\rho}_{\text{ice}}}{\rho_a} \frac{g d^2}{c_{P,a} \ell}.$$

With $g = 2{,}600$ cm s^{-2}, $\widetilde{\rho}_{\text{ice}} = 0.9$ g/cm^3, $\rho_a = 3 \times 10^{-4}$ g cm^{-3}, and $c_{P,a} = 1.4 \times 10^8$ erg g^{-1} K^{-1}, we obtain $\Delta T \sim \epsilon_{\text{drag}} \times 30$ K.

In order to estimate ϵ_{drag}, let us consider the case of a human skydiver on Earth, falling at a terminal velocity around 50 m/s. With a weight of 75 kg and a density of $\widetilde{\rho} = 1$ g/cm^3, we consider that $d \approx 50$ cm. Using parameters for the Earth at sea level, $K_a \sim 0.19$ cm^2/s, $g = 981$ cm/s^2, $\rho_a = 1.2 \times 10^{-3}$ g/cm^3, and $c_{P,a} = 1.0 \times 10^7$ erg/(g K), we obtain $\ell \sim 0.04$ cm and $\Delta T \sim \epsilon_{\text{drag}} \times 850$ K. Everyday experience does tell us that the heating should be less than a few kelvin (the same could be applied to, e.g., driving a car on the highway). Therefore $\epsilon_{\text{drag}} < 10^{-2}$, yielding a temperature increase that is negligible compared to other uncertainties.

Another way to see this is as follows: The temperature increase in the boundary layer across the mushball is proportional to gravity (2.6 times higher in Jupiter) but is inversely proportional to the product of gas density and heat capacity. At 1 bar in Jupiter, this product is similar to that at sea level on the Earth, but deeper in Jupiter, where mushballs evaporate, it is an order of magnitude higher. Therefore, the increase in temperature in the boundary layer is expected to be smaller than for a similar situation on Earth. Since everyday experience tells us that drag heating of cars on the highway or of human skydivers is small (limited to a few Kelvins at most), it must be even smaller (and therefore negligible) for mushballs in Jupiter.

A.3 Parameter Sensitivity

We have focused on a set of fiducial model parameters and a simple model to show that mushballs in Jupiter can form and potentially transport ammonia downward efficiently. In Table A1, we study how varying these parameters affect the mushballs characteristics and how far they penetrate into Jupiter's atmosphere. The pressure at which mushballs evaporate, P_{max}, their depth measured from the 1 bar level, and the fall duration are provided both for the nominal ventilation factors (Equation 9 and plain lines in Figure 3) and for 10 times lower values (dashed lines in Figure 3).

The first four lines of Table A1 correspond to our fiducial case (Figure 3), for four values of the water ice abundance, from $\widetilde{x}_{\text{H}_2\text{O}} = 100$ to 1,200 ppmv. These lead to mushballs similar to the largest hailstones on Earth, with a maximum diameter between about 10 to 18 cm and a maximum mass between 0.1 and 0.9 kg. Their maximum free-fall velocity v_{max} can reach more than 200 m/s, reaching full melting pressures P_{max} between 6.4 to over 20 bars in as much as 2.7 hr to as little as 30 min. The final NH$_3$ fraction at evaporation is always high, ensuring an efficient transport of ammonia.

When decreasing the upward velocity v_{up} to 10 m/s, the growth of mushballs is suppressed. For all but the highest H$_2$O values, they melt soon after reaching the 0°C level at pressures close to 5–6 bar. They can reach deeper levels for higher H$_2$O crystal concentrations, but the value of f_{NH_3} is then too low for an efficient transport of ammonia. Conversely, increasing v_{up} to 100 m/s leads to a fast mushball growth and a penetration depth that can reach the 27 bar level in the most favorable conditions (including a ventilation factor that is ten times lower than the nominal one).

The value of the range over which a strong updraft is present (nominally between $P_{\text{bottom}} = 5$ bar and 0.4 bar) has only a limited effect on the outcome, and results with $P_{\text{bottom}} = 2$ bar are relatively close to the nominal case. Similarly, a change of the initial seed radius of the ice crystal, $\widetilde{d}_0$, or in the relative humidity above cloud base, H_a, lead to very small changes in the final results.

Changing E_{NH_3}, the collection efficiency in the region where NH$_3 \cdot$ H$_2$O forms, leads to a limited suppression of growth for high H$_2$O ice abundances. However, for $\widetilde{x}_{\text{H}_2\text{O}} = 100$ and 300 ppmv, we notice an increase of the mushball size and penetration instead. This is because for this case, the mushball starts evaporating in a region where the updraft is still present and is transported back upward where it continues to grow. This leads to several cycles of growth and evaporation before the mushball is large enough to fall through the zone and

Table A1
Effect of Model Parameters on Mushball Characteristics and Penetration Depth

v_{up} [m/s]	P_{bottom} [bar]	$\tilde{d}_0$ [μm]	H_a	$\tilde{\rho}_{NH3}$ [g/cm^3]	$\tilde{\rho}_{H_2O}$ [g/cm^3]	E_{mush}	E_{H_2O}	E_{NH_3}	$\tilde{x}_{H_2O}$ [ppmv]	d_{max} [cm]	M_{max} [g]	v_{max} [m/s]	P_{max} [bar]	depth [km]	Duration [hr]	f_{NH_3}
50.0	5.0	100	1.0	0.3	0.3	1.0	0.3	1.0	100	6.9	63	.97	5.5–9.7	55.1–81.0	2.6–2.7	0.50
									300	9.5	166	173	6.5–12.4	62.2–93.5	1.0–1.1	0.40
									600	13.2	399	231	7.1–16.1	66.2–107.6	0.6–0.7	0.25
									1200	18.9	1093	250	8.0–21.7	71.3–125.6	0.4–0.5	0.14
10.0	5.0	100	1.0	0.3	0.3	1.0	0.3	1.0	100	1.5	1	29	5.1–6.0	52.3–58.4	1.5–1.6	0.50
									300	3.2	5	33	5.4–7.1	54.7–66.3	1.0–1.1	0.18
									600	5.4	25	43	5.8–8.6	57.4–75.0	0.7–0.9	0.07
									1200	9.4	132	140	6.4–11.6	61.9–89.8	0.5–0.7	0.02
100.0	5.0	100	1.0	0.3	0.3	1.0	0.3	1.0	100	10.6	221	341	6.4–12.1	61.7–92.0	2.2–2.3	0.50
									300	12.7	468	332	7.2–16.0	66.5–107.3	1.0–1.1	0.40
									600	18.5	1135	317	7.9–21.8	70.9–125.9	0.7–0.8	0.25
									1200	27.5	3427	330	9.0–31.0	77.1–149.5	0.4–0.6	0.14
50.0	2.0	100	1.0	0.3	0.3	1.0	0.3	1.0	100	4.8	24	97	5.8–8.1	57.2–72.4	1.7–1.8	0.50
									300	8.1	116	153	6.4–10.8	61.5–86.1	0.9–1.1	0.40
									600	12.2	325	231	7.0–15.1	65.6–104.2	0.5–0.7	0.25
									1200	17.4	849	250	7.8–19.7	70.5–119.8	0.3–0.5	0.14
50.0	5.0	30	1.0	0.3	0.3	1.0	0.3	1.0	100	6.9	65	97	5.5–9.8	55.1–81.3	3.1–3.2	0.50
									300	9.5	165	173	6.5–12.4	62.2–93.5	1.2–1.3	0.40
									600	13.4	424	245	7.2–16.3	66.6–108.5	0.7–0.8	0.25
									1200	20.1	1321	270	8.1–22.9	72.0–129.2	0.4–0.6	0.14
50.0	5.0	100	0.0	0.3	0.3	1.0	0.3	1.0	100	6.9	63	97	5.7–10.1	56.8–82.7	2.6–2.7	0.50
									300	9.5	166	173	6.6–12.7	63.1–94.6	1.0–1.1	0.40
									600	13.2	399	231	7.2–16.5	67.1–109.0	0.6–0.7	0.25
									1200	18.9	1093	250	8.1–22.2	72.2–127.1	0.4–0.5	0.14
50.0	5.0	100	1.0	0.3	0.3	1.0	0.3	0.3	100	13.1	142	132	6.4–10.6	61.6–85.3	8.1–6.5	0.50
									300	9.7	149	153	6.4–12.1	61.2–91.9	2.4–2.6	0.40
									600	12.4	312	179	6.9–14.9	65.2–103.4	1.5–1.6	0.25
									1200	17.8	895	218	7.7–20.3	69.9–121.6	0.8–1.0	0.14
50.0	5.0	100	1.0	0.1	0.1	1.0	0.3	1.0	100	14.4	180	336	5.9–9.2	58.1–78.4	1.5–1.5	0.50
									300	19.6	611	275	6.7–13.3	63.9–97.1	0.7–0.8	0.40
									600	32.8	2068	241	7.6–18.8	69.1–116.7	0.5–0.6	0.25
									1200	50.5	6914	224	8.7–26.7	75.5–139.1	0.3–0.5	0.14

fully evaporate. A full consideration of this case is beyond the scope of this paper, but it is reminiscent of hail on Earth which is known to undergo multiple episodes of growth (Pruppacher & Klett, 1997).

Finally, the last set of cases correspond to an assumed low density of both H_2O and $NH_3 \cdot H_2O$ ice. They lead to an extremely fast growth of the mushballs in less than 1.5 hr even for the low $\tilde{x}_{NH_3}$ case. Of course, these cases are extreme because compaction effects would be expected to be very significant, but they show that the assumed density of ice crystals is an important parameter. In the Earth atmosphere, graupel particles with millimeter sizes have densities ranging from 0.05 to 0.9 g cm^{-3} (see Table 2.8 of Pruppacher & Klett, 1997).

Overall, Table A1 shows that for a majority of cases, mushballs grow and deliver below the 5 bar level a mixture with a high concentration of NH_3 ($f_{NH_3} > 0.1$), in less than an hour. For all these cases, evaporative downdrafts would be expected to form and lead to a further transport of ammonia and water in the deep atmosphere. For highly favorable cases (high updraft velocities, high abundance of H_2O ice crystals and high collection rates), mushballs can penetrate deeper than the 20 bar level. However, although these may look promising to explain the Juno results directly, the evaporation of water ice takes place at levels below the water cloud where it may not be recycled efficiently. Instead, the events for which water ice evaporate mostly above the water cloud base and the mushball core is deposited below appear most favorable.

Appendix B: Nomenclature
Table B1 provides the main quantities used in this article and their default values.

Table B1
Quantities Used in This Paper

Quantity	Default value	Description
x_{NH_3}	360×10^{-6}	Volume mixing ratio of ammonia in Jupiter's deep atmosphere[a]
x_{H_2O}	2600×10^{-6}	Volume mixing ratio of water in Jupiter's deep atmosphere[b]
$\tilde{x}_{NH_3}$	-	Volume mixing ratio of condensed ammonia
$\tilde{x}_{H_2O}$	-	Volume mixing ratio of condensed water
$r_{NH_3 \cdot H_2O}$	1/2	Ratio of NH_3 to H_2O molecules in liquid $NH_3 \cdot H_2O$
$\tilde{\rho}_{H_2O}$	0.3g/cm^3	Physical density of water-ice crystals[c]
μ_{H_2O}	18 g/mol	Molar mass of H_2O
μ_{NH_3}	17 g/mol	Molar mass of NH_3
μ	2.3 g/mol	Mean molar mass in Jupiter's atmosphere
E	0.3 to 1	Collection efficiency of mushballs with ice crystals
$\tilde{d}$	-	Mushball diameter
g	$2{,}600 \text{ cm/s}^2$	Jupiter's gravitational acceleration[d]
v_{fall}	-	Terminal velocity
v_{up}	0 to 50 m/s	Updraft velocity
C_d	-	Drag coefficient
N_{Re}	-	Reynolds number
$N_{Re,crit}$	3×10^5	Critical Reynolds number above which $C_d = 0.1$
L_m	$3.34 \times 10^9 \text{erg/g}$	Latent heat of fusion of water ice[e]
L_v	$2.52 \times 10^{10} \text{erg/g}$	Latent heat of vaporization of water at 0°C[e]
P_{sat}	-	Saturation pressure of water[f]
H_a	0 to 1	Relative humidity above cloud base
$\mathscr{R}$	$8.314463 \times 10^7 \text{ erg/(mol K)}$	Gas constant
$\tilde{D}_{NH_3}^{liq}$	$10^{-5} \text{cm}^2/\text{s}$	Diffusion coefficient of ammonia in liquid water (at ~20°C)[g]
$\tilde{D}_{NH_3}^{sol}$	$4 \times 10^{-10} \text{cm}^2/\text{s}$	Diffusion coefficient of ammonia in water ice (at 140 K)[h]
$\tilde{c}_{P,H_2O}$	$1.5 \times 10^7 \text{erg/(g K)}$	Heat capacity of water ice (at −80°C)
$\tilde{k}_{H_2O}$	$3.2 \times 10^5 \text{ erg/(s cm K)}$	Thermal conductivity of water ice (at −80°C)
	Quantities varying along a Jupiter atmospheric temperature profile	
P	[1.0,17.6] bar	Atmospheric pressure[i]
T	[166.1,400.8] K	Atmospheric temperature[i]
ρ	$[1.66,12.2] \times 10^{-4} \text{g/cm}^3$	Atmospheric density[i]
z	[0,−112.9] km	Altitude from the 1 bar level[i]
v_{th}	[1.10,1.70] km/s	Thermal velocity
$c_{P,a}$	$[3.12, 3.49]\mathscr{R}$	Heat capacity of normal hydrogen[j]
η_a	$[5.97,10.9] \times 10^{-5} \text{g/(cm s)}$	Dynamic viscosity of hydrogen[j]
ν_a	$[0.41,0.10] \text{cm}^2/\text{g}$	Kinematic viscosity of hydrogen[j]
K_a	$[0.61,0.15] \text{cm}^2/\text{s}$	Thermal diffusivity of hydrogen[j]
k_a	$[1.15,2.35] \times 10^4 \text{erg/(s cm K)}$	Thermal conductivity of hydrogen[j]
D_{NH_3}	$[0.33,0.070] \text{cm}^2/\text{s}$	Diffusion coefficient of ammonia vapor in hydrogen[k]
D_{H_2O}	$[0.39,0.082] \text{cm}^2/\text{s}$	Diffusion coefficient of water vapor in hydrogen[k]
λ_{NH_3}	$[0.09,0.012] \mu\text{m}$	Mean free path of ammonia vapor in hydrogen
λ_{H_2O}	$[0.11,0.014] \mu\text{m}$	Mean free path of water vapor in hydrogen

[a]Li et al. (2017). [b]Assuming a solar N/O ratio (Lodders, 2003). [c]Approximate value based on measurement in Earth clouds (Pruppacher & Klett, 1997). [d]Value obtained using Jupiter's mean radius (Guillot, 2005). [e]https://en.wikipedia.org/wiki/Latent_heat [f]Dean (1999). [g]https://www.engineeringtoolbox.com/diffusion-coefficients-d_1404.html [h]Livingston et al. (2002). [i]Galileo probe profile (Seiff et al., 1998). [j]NIST Standard Reference Database Number 69 (https://webbook.nist.gov/chemistry/fluid/). [k]Cussler (2009).

Data Availability Statement

T.G. acknowledges support from the *Centre National d'Etudes Spatiales* and the Japan Society for the Promotion of Science. The codes used to make the figures in this paper are available online (http://doi.org/10.5281/zenodo.3749609).

References

Atreya, S. K., Wong, M. H., Owen, T. C., Mahaffy, P. R., Niemann, H. B., de Pater, I., et al. (1999). A comparison of the atmospheres of Jupiter and Saturn: Deep atmospheric composition, cloud structure, vertical mixing, and origin. *Planetary Space Science*, *47*(10-11), 1243–1262.

Becker, H., Alexander, J. W., Atreya, S. K., Bolton, S. J., Brennan, M. J., Brown, S. T., et al. (2020). Small lightning flashes from shallow electrical storms on Jupiter. *Nature*. https://doi.org/10.1038/s41586-020-2532-1

Bolton, S. J., Adriani, A., Adumitroaie, V., Allison, M., Anderson, J., Atreya, S., et al. (2017). Jupiter's interior and deep atmosphere: The initial pole-to-pole passes with the Juno spacecraft. *Science*, *356*(6340), 821–825.

Cussler, E. L. (2009). *Diffusion. Mass Transfer in Fluid Systems* (3rd ed.). Cambridge: Cambridge University Press.

Davidovits, C. R., Kolb, C. E., Williams, L. R., Jayne, J. T., & Worsnop, D. R. (2006). Mass accommodation and chemical reactions at gas-liquid interfaces. *Chemical Review*, *106*, 1323–1354.

de Pater, I., Sault, R. J., Butler, B., DeBoer, D., & Wong, M. H. (2016). Peering through Jupiter's clouds with radio spectral imaging. *Science*, *352*(6290), 1198–1201.

de Pater, I., Sault, R. J., Wong, M. H., Fletcher, L. N., DeBoer, D., & Butler, B. (2019). Jupiter's ammonia distribution derived from VLA maps at 3-37 GHz. *Icarus*, *322*, 168–191.

Dean, J. A. (1999). *Lange's handbook of chemistry* (15th ed.). New York: McGraw Hill Inc.

Gierasch, P. J., Ingersoll, A. P., Banfield, D., Ewald, S. P., Helfenstein, P., Simon-Miller, A., et al. (2000). Observation of moist convection in Jupiter's atmosphere. *Nature*, *403*(6770), 628–630.

Guillot, T. (2005). The interiors of giant planets: Models and outstanding questions. *Annual Review of Earth and Planetary Sciences*, *33*, 493–530.

Guillot, T., Miguel, Y., Militzer, B., Hubbard, W. B., Kaspi, Y., Galanti, E., et al. (2018). A suppression of differential rotation in Jupiter's deep interior. *Nature*, *555*(7695), 227–230.

Homann, H., Guillot, T., Bec, J., Ormel, C. W., Ida, S., & Tanga, P. (2016). Effect of turbulence on collisions of dust particles with planetesimals in protoplanetary disks. *Astronomy and Astrophysics*, *589*, A129.

Hueso, R., Sánchez-Lavega, A., & Guillot, T. (2002). A model for large-scale convective storms in Jupiter. *Journal of Geophysical Research*, *107*(E10), 5075. https://doi.org/10.1029/2001JE001839

Ingersoll, A. P., Adumitroaie, V., Allison, M. D., Atreya, S., Bellotti, A. A., Bolton, S. J., et al. (2017). Implications of the ammonia distribution on Jupiter from 1 to 100 bars as measured by the Juno microwave radiometer. *Geophysical Research Letters*, *44*, 7676–7685. https://doi.org/10.1002/2017GL074277

Jin, R., & Chu, L. T. (2007). Uptake of NH3 and NH3+ HOBr Reaction on Ice Surfaces at 190 K. *Journal of Physical Chemistry A*, *111*(32), 7833–7840.

Kargel, J. S. (1992). Ammonia-water volcanism on icy satellites: Phase relations at 1 atmosphere. *Icarus*, *100*(2), 556–574.

Kargel, J. S., Croft, S. K., Lunine, J. I., & Lewis, J. S. (1991). Rheological properties of ammonia-water liquids and crystal-liquid slurries: Planetological applications. *Icarus*, *89*(1), 93–112.

Kasper, T., Wong, M. H., Marschall, J., de Pater, I., Romani, P. N., & Kalogerakis, K. S. (2011). Uptake of ammonia gas by Jovian ices. *EPSC-DPS joint meeting 2011* (Vol. 6, pp. 352).

Kessler, E. (1969). On the distribution and continuity of water substance in atmospheric circulation. *Meteorological monographs* (Vol. 10, pp. 1–84). Boston, MA: American Meteorological Society.

Kundu, P. K., & Cohen, I. M. (2016). *Fluid mechanics: Sixth edition*. Amsterdam: Academic Press.

Lewis, J. S. (1969). The clouds of Jupiter and the NH_3, H_2O and $NH_3.H_2S$ systems. *Icarus*, *10*(3), 365–378.

Li, C., Ingersoll, A., Bolton, S., Levin, S., Janssen, M., Atreya, S., et al. (2020). The water abundance in Jupiter's equatorial zone. *Nature Astronomy*, *4*(6), 609–616. https://doi.org/10.1038/s41550-020-1009-3

Li, C., Ingersoll, A., Janssen, M., Levin, S., Bolton, S., Adumitroaie, V., et al. (2017). The distribution of ammonia on Jupiter from a preliminary inversion of Juno microwave radiometer data. *Geophysical Research Lettters*, *44*, 5317–5325. https://doi.org/10.1002/2017GL073159

Livingston, F. E., Smith, J. A., & George, S. M. (2002). General trends for bulk diffusion in ice and surface diffusion on ice. *Journal of Physical Chemistry A*, *106*(26), 6309–6318.

Lodders, K. (2003). Solar system abundances and condensation temperatures of the elements. *Astrophysical Journal*, *591*(2), 1220–1247.

Nelson, S. P. (1983). The influence of storm flow structure on hail growth. *Journal of Atmospheric Sciences*, *40*(8), 1965–1983.

Phillips, V. T. J., Formenton, M., Bansemer, A., Kudzotsa, I., & Lienert, B. (2015). A parameterization of sticking efficiency for collisions of snow and graupel with ice crystals: Theory and comparison with observations*. *Journal of Atmospheric Sciences*, *72*(12), 4885–4902.

Pruppacher, H. R., & Klett, J. D. (1997). *Microphysics of clouds and precipitation* (pp. 2). Dordrecht: Kluwer Academic Publishers.

Rasmussen, R. M., & Heymsfield, A. J. (1987). Melting and shedding of graupel and hail. Part I: Model physics. *Journal of Atmospheric Sciences*, *44*(19), 2754–2763.

Rasmussen, R. M., Levizzani, V., & Pruppacher, H. R. (1984). A wind tunnel and theoretical study on the melting behavior of atmospheric ice particles: III. Experiment and theory for spherical ice particles of radius larger than 500 microns. *Journal of Atmospheric Sciences*, *41*(3), 381–388.

Rogers, R. R., & Yau, M. K. (1996). *A short course in cloud physics*. Elsevier.

Roos, D. V. D. S. (1972). A giant hailstone from Kansas in free fall. *Journal of Applied Meteorology*, *11*(6), 1008–1011.

Seiff, A., Kirk, D. B., Knight, T. C. D., Young, R. E., Mihalov, J. D., Young, L. A., et al. (1998). Thermal structure of Jupiter's atmosphere near the edge of a 5-μm hot spot in the north equatorial belt. *Journal Geophysical Research*, *103*(E10), 22,857–22,890.

Showman, A. P., & de Pater, I. (2005). Dynamical implications of Jupiter's tropospheric ammonia abundance. *Icarus*, *174*(1), 192–204.

Stein, R. F., & Nordlund, Å. (1998). Simulations of solar granulation. I. General Properties. *The Astrophysical Journal*, *499*(2), 914–933.

Stoker, C. R. (1986). Moist convection: A mechanism for producing the vertical structure of the Jovian Equatorial Plumes. *Icarus*, *67*(1), 106–125.

Sugiyama, K., Nakajima, K., Odaka, M., Kuramoto, K., & Hayashi, Y. Y. (2014). Numerical simulations of Jupiter's moist convection layer: Structure and dynamics in statistically steady states. *Icarus*, *229*, 71–91.

Turner, J. S. (1969). Buoyant plumes and thermals. *Annual Review of Fluid Mechanics*, *1*(1), 29–44.

Weidenschilling, S. J., & Lewis, J. S. (1973). Atmospheric and cloud structures of the Jovian planets. *Icarus*, *20*(4), 465–476.

Yair, Y., Levin, Z., & Tzivion, S. (1995). Microphysical processes and dynamics of a Jovian thundercloud. *Icarus*, *114*(2), 278–299.